# First-Principles Diffusivity Ratios for Atmospheric Isotope Fractionation on Mars and Titan

**Robert Hellmann**[1], **Allan H. Harvey**[2]

[1]Institut für Thermodynamik, Helmut-Schmidt-Universität / Universität der Bundeswehr Hamburg, Holstenhofweg 85, 22043 Hamburg, Germany

[2]Applied Chemicals and Materials Division, National Institute of Standards and Technology, 325 Broadway, Boulder, Colorado 80305, U.S.A.

**Key Points:**

- Kinetic isotope fractionation depends on diffusivity ratios that have not been measured for conditions corresponding to Mars or Titan.
- The relative diffusivity of isotopologues can be calculated as a function of temperature from high-accuracy intermolecular potentials.
- Rigorous results agree well with simpler kinetic theory for water on Mars, but less well for methane on Titan.

Corresponding author: Robert Hellmann, robert.hellmann@hsu-hh.de

**Abstract**

Recent work used the kinetic theory of molecular gases, along with state-of-the-art intermolecular potentials, to calculate from first principles the diffusivity ratios necessary for modeling kinetic fractionation of water isotopes in air. Here, we extend that work to the Martian atmosphere, employing potential-energy surfaces for the interaction of water with carbon dioxide and with nitrogen. We also derive diffusivity ratios for methane isotopes in the atmosphere of Titan by using a high-quality potential for the methane-nitrogen pair. The Mars calculations cover 100 K to 400 K, while the Titan calculations cover 50 K to 200 K. Surprisingly, the simple hard-sphere theory that is inaccurate for Earth's atmosphere is in good agreement with the rigorous results for the diffusion of water isotopes in the Martian atmosphere. A modest disagreement with the hard-sphere results is observed for the diffusivity ratio of $CH_3D$ in the atmosphere of Titan. We present temperature-dependent correlations, as well as estimates of uncertainty, for the diffusivity ratios involving HDO, $H_2{}^{17}O$, and $H_2{}^{18}O$ in the Martian atmosphere, and for $CH_3D$ and $^{13}CH_4$ in the atmosphere of Titan, providing for the first time the necessary data to be able to model kinetic isotope fractionation in these environments.

## Plain Language Summary

Different isotopes distribute unevenly between the vapor phase and liquid or solid phases during precipitation and evaporation, and the resulting changes in isotope ratios are used in the study of climate and other geophysical processes. While equilibrium aspects of this fractionation are fairly well understood, in some circumstances there is also a kinetic component that depends on the relative diffusivities of different isotopic species in the atmosphere. We used rigorous molecular collision calculations to model this effect for water isotopes in the $CO_2$-rich Martian atmosphere and for methane isotopes in the nitrogen atmosphere of Titan. For the Martian atmosphere, the results are not significantly different from those obtained by a simple theory that assumes the molecules to be hard spheres; this is surprising since previous work showed that the hard-sphere approach is significantly in error for water in Earth's atmosphere. For methane in the atmosphere of Titan, a small improvement is obtained for the diffusivity ratio of $CH_3D$. We provide simple correlations that allow these diffusivity ratios to be used in planetary modeling.

## 1 Introduction

On Earth, the fractionation of stable water isotopes such as HDO and $H_2{}^{18}O$ is important for understanding the hydrologic cycle (Gat, 1996). In addition to the equilibrium fractionation that occurs between water vapor and ice or liquid water, in some cases a significant role is played by kinetic fractionation that depends on the ratio of the atmospheric diffusivity of the isotopologue of interest to that of $H_2O$. Recently, we reported temperature-dependent diffusivity ratios in air calculated from the kinetic theory of molecular gases applied to state-of-the-art intermolecular potentials based on *ab initio* calculations for the interaction between water and molecular nitrogen and oxygen (Hellmann & Harvey, 2020). We found that, especially for HDO, the often-assumed constant diffusivity ratios from simple hard-sphere kinetic theory were in error, and that the temperature dependence of the diffusivity ratios was not negligible. We supplied recommended diffusivity ratios and their uncertainties from 190 K to 500 K, greatly exceeding the range in which the (scattered) experimental data exist.

Earth is not the only place in our solar system with a hydrologic cycle. The distribution and seasonal variation of isotopic water species (especially HDO) has been used to study the climate of Mars (Montmessin et al., 2005; Villanueva et al., 2015; Krasnopolsky, 2015; Encrenaz et al., 2016; Vos et al., 2019). Current modeling of isotopic cycles on Mars neglects kinetic fractionation (Montmessin et al., 2005). To our knowledge, no

experimental measurements of the relevant diffusivity ratios exist. Based on our results for Earth's atmosphere (Hellmann & Harvey, 2020), a hard-sphere estimate for the diffusivity ratios would be expected to be in error. Because the Martian atmosphere consists primarily of carbon dioxide, diffusivity ratios in terrestrial air are not applicable, requiring new calculations.

Another "hydrologic" cycle of interest is found on Titan, where methane precipitates in a nitrogen atmosphere (Roe, 2012; Mitchell & Lora, 2016; Hayes et al., 2018). There has been some study of methane isotopes (especially $CH_3D$) in the atmosphere of Titan (Nixon et al., 2012; Ádámkovics & Mitchell, 2016; Hörst, 2017; Thelen et al., 2019). Information exists on equilibrium fractionation of $CH_3D$ (Armstrong et al., 1955; Calado et al., 1997), but the relative diffusivities have not been studied. While we are unaware of any current plans to include kinetic fractionation in models of Titan's atmosphere, we calculate the diffusivity ratios so that they will be available if needed.

We follow the notation of Hellmann and Harvey (2020) in defining the relative diffusivities for water isotopologues as $D_{\mathrm{r,HDO}} \equiv D_{\mathrm{HDO}}/D_{\mathrm{H_2O}}$, $D_{\mathrm{r},17} \equiv D_{\mathrm{H_2{}^{17}O}}/D_{\mathrm{H_2O}}$, and $D_{\mathrm{r},18} \equiv D_{\mathrm{H_2{}^{18}O}}/D_{\mathrm{H_2O}}$, where $D_i$ is the diffusivity of species $i$ in the atmosphere of interest. Similarly, for the diffusion ratios for methane, $D_{\mathrm{r,CH_3D}} \equiv D_{\mathrm{CH_3D}}/D_{\mathrm{CH_4}}$ and $D_{\mathrm{r},13} \equiv D_{\mathrm{{}^{13}CH_4}}/D_{\mathrm{CH_4}}$.

For hard spheres at low density, simple kinetic theory yields

$$D_{\mathrm{r},i} = \left[\frac{M_0(M_i + M_\mathrm{G})}{M_i(M_0 + M_\mathrm{G})}\right]^{1/2} \tag{1}$$

for the ratio of the diffusivity of an isotopic species $i$ to that of the reference species (subscript 0) in a gas G, where $M$ is the molar mass. In this relation, the diameters of the isotopic species and of the reference species are assumed to be equal. If minor components (those other than $CO_2$, $N_2$, and Ar) are ignored, the composition of the Martian atmosphere (Trainer et al., 2019) yields a molar mass of 43.5 $\mathrm{g\,mol^{-1}}$, and for Titan we use the molar mass of $N_2$, which is 28.0134 $\mathrm{g\,mol^{-1}}$. In this simplification, Equation 1 yields for the Martian atmosphere 0.9811 for $D_{\mathrm{r,HDO}}$, 0.9812 for $D_{\mathrm{r},17}$, and 0.9640 for $D_{\mathrm{r},18}$. For a nitrogen atmosphere (Titan), the result is 0.9811 for $D_{\mathrm{r,CH_3D}}$ and 0.9813 for $D_{\mathrm{r},13}$. [After our calculations were completed, it was brought to our attention that molar masses slightly different from these terrestrial values would have been appropriate, due to different isotopic compositions on Mars and Titan. For example, $N_2$ on Titan has more $^{15}N$ than on Earth (Niemann et al., 2010), leading to a molar mass of 28.018 g $\mathrm{mol^{-1}}$. These differences are negligible in the context of the present calculations.]

As shown by Hellmann and Harvey (2020), the simple hard-sphere kinetic theory is inaccurate for water, because it ignores the rotational dynamics that are affected by isotopic substitution (especially H/D substitution). Modern kinetic theory can significantly improve on the hard-sphere results. The relevant collision integrals (sometimes called generalized cross sections) can be calculated essentially exactly from the full intermolecular potential-energy surface. In this work, we use state-of-the-art pair potentials for the $H_2O$–$CO_2$ and $H_2O$–$N_2$ interactions to calculate the diffusivity ratios $D_{\mathrm{r,HDO}}$, $D_{\mathrm{r},17}$, and $D_{\mathrm{r},18}$ in the Martian atmosphere as a function of temperature. Similarly, we use a high-accuracy potential for the $CH_4$–$N_2$ interaction to calculate $D_{\mathrm{r,CH_3D}}$ and $D_{\mathrm{r},13}$ at conditions relevant to Titan.

## 2 Methods and Results

### 2.1 Intermolecular Potentials

The pair potentials used in this work for modeling $H_2O$–$CO_2$ (Hellmann, 2019a), $H_2O$–$N_2$ (Hellmann, 2019b), and $CH_4$–$N_2$ (Hellmann et al., 2014) interactions were developed using state-of-the-art quantum-chemical *ab initio* approaches, see these papers

**Table 1.** Zero-Point Vibrationally Averaged Geometries of $H_2O$, HDO, $D_2O$, $H_2{}^{17}O$, and $H_2{}^{18}O$ in Terms of the Bond Lengths $r_{OX}$ (with X=H or X=D) and the Bond Angle $\theta$ from Quantum-Chemical Cubic Force Field Calculations at the Frozen-Core CCSD(T)/cc-pVQZ Level of Theory, as Reported by Hellmann and Harvey (2020)

| Isotopologue | Geometric Parameter | Value | Deviation from $H_2O$ |
|---|---|---|---|
| $H_2O$ | $r_{OH}$ | 97.262 pm | |
| | $\theta$ | 104.00° | |
| HDO | $r_{OH}$ | 97.126 pm | −0.135 pm |
| | $r_{OD}$ | 96.947 pm | −0.315 pm |
| | $\theta$ | 104.01° | 0.01° |
| $D_2O$ | $r_{OD}$ | 96.861 pm | −0.401 pm |
| | $\theta$ | 104.00° | 0.00° |
| $H_2{}^{17}O$ | $r_{OH}$ | 97.259 pm | −0.003 pm |
| | $\theta$ | 104.00° | 0.00° |
| $H_2{}^{18}O$ | $r_{OH}$ | 97.257 pm | −0.005 pm |
| | $\theta$ | 104.00° | 0.00° |

for full details. We used the potentials without modifications for the calculations with HDO, $H_2{}^{17}O$, $H_2{}^{18}O$, $CH_3D$, and $^{13}CH_4$. This is a valid approximation only if the isotopic substitutions of water and methane affect the collisional dynamics predominantly through the changes to the molecular masses and to the moment of inertia tensors and not through changes to the pair potential-energy surfaces. Here, we provide justifications for this assumption.

If the geometries of HDO, $H_2{}^{17}O$, and $H_2{}^{18}O$ were identical to that of $H_2O$ and the geometries of $CH_3D$ and $^{13}CH_4$ were identical to that of $CH_4$, the respective interaction potentials would also be identical apart from very small effects beyond the Born–Oppenheimer approximation. While the equilibrium geometries are indeed identical (at least within the Born–Oppenheimer approximation), the zero-point vibrationally averaged geometries, which better represent the molecules in a rigid-rotor treatment of thermophysical properties, are not. For the development of the $H_2O$–$CO_2$, $H_2O$–$N_2$, and $CH_4$–$N_2$ pair potentials, vibrationally averaged geometries of $H_2O$ and $CH_4$ were used.

The changes in the vibrationally averaged molecular geometries for the three different isotopic substitutions of $H_2O$ were obtained in our previous work (Hellmann & Harvey, 2020) from cubic force field calculations at the frozen-core CCSD(T)/cc-pVQZ level of theory using the CFOUR quantum chemistry code (Stanton et al., 2019). For convenience, the results are provided here again, see Table 1. Only the geometry of HDO changes appreciably, with the OH bond length differing by −0.14% and the OD bond length differing by −0.32% from the OH bond length in $H_2O$. In the present work, we performed a similar analysis of the geometries of the $CH_4$ isotopologues at the frozen-core CCSD(T)/cc-pVTZ level using CFOUR. The results are shown in Table 2. While the geometry of $^{13}CH_4$ is virtually identical to that of $CH_4$, the lengths of the three CH bonds and the single CD bond in $CH_3D$ differ by −0.08% and −0.17%, respectively, from the length of the CH bonds in $CH_4$.

To take the differing bond lengths between $H_2O$ and HDO properly into account, one would have to compute the differences in the interaction energies with $CO_2$ and $N_2$ between the two geometries in order to construct dedicated HDO–$CO_2$ and HDO–$N_2$ potentials, but this is quite complicated due to the lower symmetry of HDO. However, this complication does not occur with $D_2O$, whose bonds are 0.41% shorter than those of $H_2O$

**Table 2.** Zero-Point Vibrationally Averaged Geometries of $CH_4$, $CH_3D$, $CD_4$, and $^{13}CH_4$ in Terms of the Bond Lengths $r_{CX}$ (with X=H or X=D) and the Bond Angles $\theta_{XCY}$ (with X=H or X=D and Y=H or Y=D), as Obtained from Quantum-Chemical Cubic Force Field Calculations at the Frozen-Core CCSD(T)/cc-pVTZ Level of Theory

| Isotopologue | Geometric Parameter | Value | Deviation from $CH_4$ |
|---|---|---|---|
| $CH_4$ | $r_{CH}$ | 110.209 pm | |
| | $\theta_{HCH}$ | 109.47° | |
| $CH_3D$ | $r_{CH}$ | 110.122 pm | −0.087 pm |
| | $r_{CD}$ | 110.018 pm | −0.192 pm |
| | $\theta_{HCH}$ | 109.48° | 0.01° |
| | $\theta_{HCD}$ | 109.46° | −0.01° |
| $CD_4$ | $r_{CD}$ | 109.853 pm | −0.356 pm |
| | $\theta_{DCD}$ | 109.47° | 0.00° |
| $^{13}CH_4$ | $r_{CH}$ | 110.206 pm | −0.003 pm |
| | $\theta_{HCH}$ | 109.47° | 0.00° |

(see Table 1). Calculations of $D_{D_2O/CO_2}$ with both the $H_2O$–$CO_2$ potential and a dedicated $D_2O$–$CO_2$ potential derived from it would thus be a suitable proxy for estimating the influence of the water geometry, an approach that we already applied in our previous work (Hellmann & Harvey, 2020) for the interactions with $N_2$. Therefore, we constructed a $D_2O$–$CO_2$ potential by first computing the differences in the interaction energies due to the differences between the $D_2O$ and $H_2O$ geometries at the reasonably accurate RI-MP2/aug-cc-pVQZ (plus bond functions) level of theory using the ORCA program (Neese, 2012); see Hellmann (2019a) for more details on these types of calculations. In the next step, we added these differences to the $H_2O$–$CO_2$ interaction energies of Hellmann (2019a) and refitted the potential. Kinetic-theory calculations of $D_{D_2O/CO_2}$ with the two potentials yielded values that differ by only 0.13% at 100 K, 0.11% at 200 K, and again 0.13% at 400 K, with the values for the $D_2O$–$CO_2$ potential being consistently larger. For $D_{HDO/CO_2}$, the effect is expected to be only about half as large.

For $CH_3D$ in $N_2$, the complications are similar due to the lower symmetry of $CH_3D$ compared with $CH_4$. Using $CD_4$ to estimate the influence of the different geometries circumvents these problems. The bonds in $CD_4$ are 0.32% shorter than those in $CH_4$ (see Table 2). We constructed a $CD_4$–$N_2$ potential by calculating the differences in the interaction energies resulting from the differences between the $CD_4$ and $CH_4$ geometries at the frozen-core CCSD(T)/aug-cc-pVTZ [plus bond functions, see Hellmann et al. (2014) for details] level of theory using the CFOUR program. The further steps are analogous to the $D_2O$–$CO_2$ case. The differences between the $D_{CD_4/N_2}$ values obtained with the $CD_4$–$N_2$ and $CH_4$–$N_2$ potentials are 0.24% at 50 K, 0.23% at 100 K, and 0.18% at 200 K, with the values for the $CD_4$–$N_2$ potential being always larger. With only one CD bond in $CH_3D$, the respective differences for $D_{CH_3D/N_2}$ should be roughly four times smaller.

Thus, we can conclude that the errors introduced by using the pair potentials without further adjustments likely do not exceed 0.1% for both $D_{r,HDO}$ and $D_{r,CH_3D}$ and are completely negligible for $D_{r,17}$, $D_{r,18}$, and $D_{r,13}$. A similar analysis with similar conclusions was presented in our work on water diffusivity ratios in Earth's atmosphere (Hellmann & Harvey, 2020). An important advantage of using the same pair potentials for different isotopologues is that any inaccuracies in the potentials that would cause $D_{H_2O}$ and $D_{CH_4}$ to be in error would affect $D$ for the substituted isotopologues in a similar manner, making the diffusivity ratios insensitive to such errors.

### 2.2 Kinetic-Theory Calculations

The kinetic-theory calculations performed in this work are only briefly summarized here. The interested reader is referred to Hellmann (2019a, 2019b) and Hellmann et al. (2014) for more detailed descriptions of the methodology.

The required collision integrals (generalized cross sections) for computing the diffusivity ratios were obtained from classical trajectories for binary collisions of $H_2O$, HDO, $H_2{}^{17}O$, and $H_2{}^{18}O$ with $CO_2$ and $N_2$ and of $CH_4$, $CH_3D$, and $^{13}CH_4$ with $N_2$. Rigid molecules were assumed, and the trajectories were calculated from Hamilton's equations solved numerically from pre-collisional to post-collisional asymptotic conditions. For a given constant collision energy, the generalized cross sections are expressed as 11-dimensional integrals over the initial states of the trajectories, which are characterized by the spatial orientations of the two molecules, their angular momentum vectors, and the impact parameter (the intermolecular separation at closest approach if there were no interactions between the molecules). This high dimensionality necessitated using a Monte Carlo integration approach, involving, for each collision energy, the computation of typically several million trajectories. An appropriate thermal averaging procedure was used to convert the generalized cross sections at fixed collision energies to values as a function of temperature, from which the diffusivities can be obtained in a straightforward manner. The range of investigated collision energies was chosen such that the diffusivities of the $H_2O$ and $CH_4$ isotopes could be obtained at temperatures as low as 100 K and 50 K, respectively. The computations of the generalized cross sections at different energies (and temperatures) were performed with an in-house version of the TRAJECT code (Heck & Dickinson, 1996). Unlike the original program, our version is not limited to linear molecules.

The diffusivities were calculated for mole fractions of water and methane approaching zero. For the atmospheres of Mars and Titan, this is a sensible choice, which has the additional advantage that in this limit the diffusivities depend only on the interaction potentials between unlike species. Thus, no models were needed for $H_2O$–$H_2O$, $CH_4$–$CH_4$, $CO_2$–$CO_2$, and $N_2$–$N_2$ interactions. We note that the mole-fraction dependencies of the diffusivities do not exceed a few tenths of a percent at any temperature; this small effect would almost completely vanish in the diffusivity ratios.

To obtain the diffusivities of water isotopes in Mars' atmosphere, the respective diffusivities in $CO_2$ and $N_2$ were weighted with the use of a result from first-order kinetic theory (Marrero & Mason, 1972),

$$D_i = \left( \frac{x_{\mathrm{CO_2}}}{D_{i/\mathrm{CO_2}}} + \frac{x_{\mathrm{N_2}}}{D_{i/\mathrm{N_2}}} \right)^{-1}, \tag{2}$$

where the mole fraction of $CO_2$ is $x_{\mathrm{CO_2}} = 0.9545$ (Trainer et al., 2019) and that of $N_2$ accounts also for argon and all other minor components, so that $x_{\mathrm{N_2}} = 1 - x_{\mathrm{CO_2}}$. This simplification is justified because the diffusivity of water vapor is very similar in argon and in nitrogen (O'Connell et al., 1969).

The calculated diffusivity ratios $D_{\mathrm{r,HDO}}$, $D_{\mathrm{r},17}$, and $D_{\mathrm{r},18}$ in the Martian atmosphere are given for selected temperatures up to 400 K in Table 3 and are shown graphically in Figure 1, while the calculated ratios $D_{\mathrm{r,CH_3D}}$ and $D_{\mathrm{r},13}$ in $N_2$ are provided at selected temperatures up to 200 K in Table 4 and are shown in Figure 2. The ratios have expanded statistical uncertainties ($k = 2$, roughly equivalent to a 95% confidence interval) of less than 0.1% and 0.05% for the atmospheres of Mars and Titan, respectively. This uncertainty component arises from the Monte Carlo integration over the randomly chosen initial conditions of the trajectories for the binary collisions. The expanded uncertainties listed in the tables and displayed in the figures also take into account that we neglected the influence of isotopic substitutions on the pair potentials and that quantum effects on the generalized cross sections are not accounted for due to calculating the collision trajectories classically.

The quantum effects on the collision integrals depend not only on the pair potential and temperature, but also on the masses and moments of inertia of the two colliding molecules, so they will not fully cancel out in the diffusivity ratios. Our estimates for the magnitude of quantum effects are educated guesses based on our experience. Support for our estimates comes, for example, from the fact that the viscosity of dilute water vapor obtained from classical calculations such as those performed here for $H_2O$–$H_2O$ collisions differs from reliable experimental data near room temperature by less than 1% (Hellmann & Vogel, 2015). Although viscosity and diffusivity in dilute gases are closely related quantities for which quantum effects should be roughly similar on a relative scale, the $H_2O$–$H_2O$ system is quite different from those considered here, and our lowest temperatures are significantly below those of the water data. However, we can draw some insight from the second virial coefficient, which is a thermophysical property that, like the dilute-gas viscosity and diffusivity, is determined solely by pair interactions. Quantum effects are much more important for second virial coefficients than for diffusivities, so we cannot directly compare their influence on the two properties. But a comparison of the relative magnitudes of the quantum effects on the second virial coefficient of water at ambient temperature with those on the second virial coefficients of the $H_2O$–$CO_2$ and $CH_4$–$N_2$ systems at our lowest temperatures should provide a qualitative measure of the quantum character of these systems. For water, quantum effects change the second virial coefficient at 300 K by about 20% (Garberoglio et al., 2018), while for $H_2O$–$CO_2$ at 100 K and $CH_4$–$N_2$ at 50 K the changes [calculated semiclassically as done by Hellmann (2019a) and Hellmann et al. (2014)] are about 44% and 12%, respectively. Thus, by this rough measure, the $H_2O$–$CO_2$ system at 100 K can be said to have a stronger quantum character than the $H_2O$–$H_2O$ system at 300 K, but this is taken into account in our uncertainty estimates, which we believe to be conservative.

Table S1 of the supporting information provides the calculated absolute diffusivities of $H_2O$, HDO, $H_2{}^{17}O$, and $H_2{}^{18}O$ in $CO_2$, $N_2$, and Mars' atmosphere at a large number of temperatures from 100 K to 1000 K, normalized to a standard pressure of 101.325 kPa (1 atm). For $CH_4$, $CH_3D$, and $^{13}CH_4$ in $N_2$, the respective diffusivities are provided from 50 K to 500 K in Table S2. Note that the diffusivities of $H_2O$ in $CO_2$ and $N_2$ at several temperatures from 250 K to 1000 K and the diffusivities of $CH_4$ in $N_2$ from 70 K to 500 K were previously provided by Hellmann (2019a, 2019b) and Hellmann et al. (2014) and are only listed here for convenience.

## 3 Discussion

The results shown in Figure 1 for water isotopes on Mars are surprising, in that they show good agreement between our rigorous kinetic-theory calculations and the results from a simple hard-sphere calculation. That was clearly not the case for water isotopes in Earth's atmosphere, as can be seen in Figure 3 which we reproduce from the paper of Hellmann and Harvey (2020). In air, $D_{\mathrm{r,HDO}}$ differs from unity by roughly 50% more than does the hard-sphere result, and displays a clear temperature dependence; $D_{\mathrm{r},18}$ differs less dramatically from the hard-sphere result but the difference is still significant compared to the uncertainty of the calculations. In that previous work (Hellmann & Harvey, 2020), we attributed the failure of the hard-sphere approach to the significant anisotropy of the $H_2O$–$N_2$ and $H_2O$–$O_2$ interactions and to the degree to which isotopic substitution changes the rotational dynamics. The results for Mars are dominated by the $H_2O$–$CO_2$ interaction, where these factors in the collision dynamics should be at least as large as for $H_2O$ with the components of air. It therefore seems likely that there are compensating effects that cause the net diffusivity ratios for $H_2O$–$CO_2$ to be similar to the hard-sphere results. There is some deviation from the hard-sphere result for $D_{\mathrm{r,HDO}}$ at the lowest temperatures examined, but the difference is within the uncertainty of our calculations. Our results for $D_{\mathrm{r},18}$ show a temperature dependence that seems to be (barely) significant compared to the uncertainties of the calculations.

**Table 3.** Calculated Diffusivity Ratios for Water Isotopologues in Mars' Atmosphere at Selected Temperatures and Estimates of Their Expanded Uncertainties at the 95% Confidence Level

| $T$/K | $D_{\mathrm{r,HDO}}$ | $D_{\mathrm{r},17}$ | $D_{\mathrm{r},18}$ |
|---|---|---|---|
| 100 | 0.9772 ± 0.0100 | 0.9797 ± 0.0020 | 0.9615 ± 0.0040 |
| 110 | 0.9779 ± 0.0093 | 0.9796 ± 0.0020 | 0.9614 ± 0.0038 |
| 120 | 0.9785 ± 0.0086 | 0.9796 ± 0.0019 | 0.9613 ± 0.0036 |
| 130 | 0.9791 ± 0.0079 | 0.9795 ± 0.0019 | 0.9612 ± 0.0034 |
| 140 | 0.9797 ± 0.0072 | 0.9795 ± 0.0018 | 0.9612 ± 0.0032 |
| 150 | 0.9802 ± 0.0065 | 0.9795 ± 0.0018 | 0.9613 ± 0.0030 |
| 160 | 0.9806 ± 0.0058 | 0.9796 ± 0.0017 | 0.9614 ± 0.0028 |
| 170 | 0.9810 ± 0.0051 | 0.9796 ± 0.0017 | 0.9615 ± 0.0026 |
| 180 | 0.9813 ± 0.0044 | 0.9797 ± 0.0016 | 0.9617 ± 0.0024 |
| 190 | 0.9815 ± 0.0037 | 0.9798 ± 0.0016 | 0.9619 ± 0.0022 |
| 200 | 0.9816 ± 0.0030 | 0.9799 ± 0.0015 | 0.9621 ± 0.0020 |
| 220 | 0.9818 ± 0.0027 | 0.9801 ± 0.0014 | 0.9626 ± 0.0018 |
| 240 | 0.9818 ± 0.0024 | 0.9803 ± 0.0013 | 0.9630 ± 0.0016 |
| 260 | 0.9818 ± 0.0021 | 0.9806 ± 0.0012 | 0.9635 ± 0.0014 |
| 280 | 0.9816 ± 0.0018 | 0.9808 ± 0.0011 | 0.9639 ± 0.0012 |
| 300 | 0.9815 ± 0.0015 | 0.9811 ± 0.0010 | 0.9643 ± 0.0010 |
| 350 | 0.9811 ± 0.0015 | 0.9816 ± 0.0010 | 0.9652 ± 0.0010 |
| 400 | 0.9806 ± 0.0015 | 0.9820 ± 0.0010 | 0.9659 ± 0.0010 |

**Table 4.** Calculated Diffusivity Ratios for Methane Isotopologues in Nitrogen at Selected Temperatures and Estimates of Their Expanded Uncertainties at the 95% Confidence Level

| $T$/K | $D_{\mathrm{r,CH_3D}}$ | $D_{\mathrm{r},13}$ |
|---|---|---|
| 50 | 0.9775 ± 0.0040 | 0.9818 ± 0.0020 |
| 55 | 0.9776 ± 0.0038 | 0.9816 ± 0.0019 |
| 60 | 0.9777 ± 0.0036 | 0.9815 ± 0.0018 |
| 65 | 0.9779 ± 0.0034 | 0.9814 ± 0.0017 |
| 70 | 0.9780 ± 0.0032 | 0.9813 ± 0.0016 |
| 75 | 0.9783 ± 0.0030 | 0.9813 ± 0.0015 |
| 80 | 0.9785 ± 0.0028 | 0.9812 ± 0.0014 |
| 85 | 0.9787 ± 0.0026 | 0.9812 ± 0.0013 |
| 90 | 0.9790 ± 0.0024 | 0.9811 ± 0.0012 |
| 95 | 0.9792 ± 0.0022 | 0.9811 ± 0.0011 |
| 100 | 0.9794 ± 0.0020 | 0.9811 ± 0.0010 |
| 110 | 0.9799 ± 0.0018 | 0.9811 ± 0.0009 |
| 120 | 0.9802 ± 0.0016 | 0.9811 ± 0.0008 |
| 130 | 0.9806 ± 0.0014 | 0.9810 ± 0.0007 |
| 140 | 0.9809 ± 0.0012 | 0.9810 ± 0.0006 |
| 160 | 0.9813 ± 0.0010 | 0.9810 ± 0.0005 |
| 180 | 0.9817 ± 0.0010 | 0.9810 ± 0.0005 |
| 200 | 0.9819 ± 0.0010 | 0.9810 ± 0.0005 |

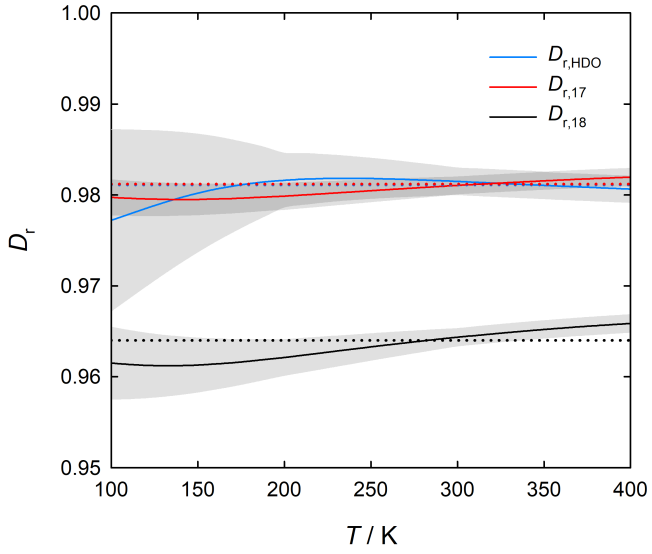


**Figure 1.** Calculated diffusivity ratios $D_{\mathrm{r,HDO}}$, $D_{\mathrm{r},17}$, and $D_{\mathrm{r},18}$ in the atmosphere of Mars as a function of temperature. The shaded areas indicate the estimated expanded uncertainty of the calculations at the 95% confidence level. The dotted horizontal lines correspond to the diffusivity ratios resulting from the simple hard-sphere kinetic theory, Equation 1.

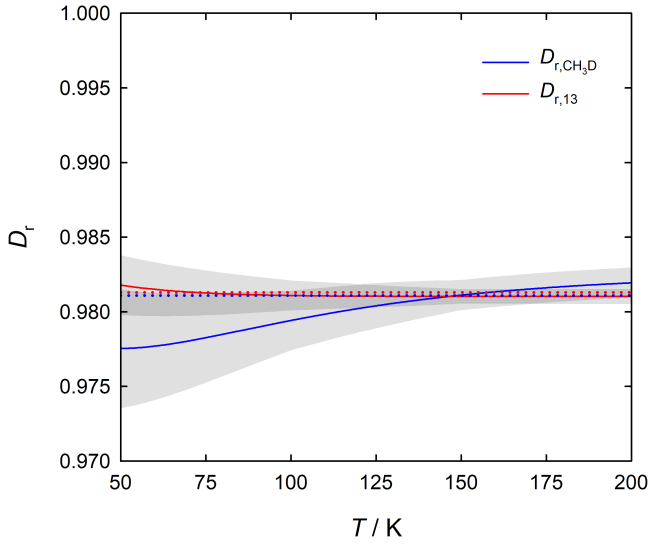


**Figure 2.** Calculated diffusivity ratios $D_{\mathrm{r},\mathrm{CH_3D}}$ and $D_{\mathrm{r},13}$ in $N_2$ as a function of temperature. The shaded areas indicate the estimated expanded uncertainty of the calculations at the 95% confidence level. The dotted horizontal lines correspond to the diffusivity ratios resulting from the simple hard-sphere kinetic theory, Equation 1.

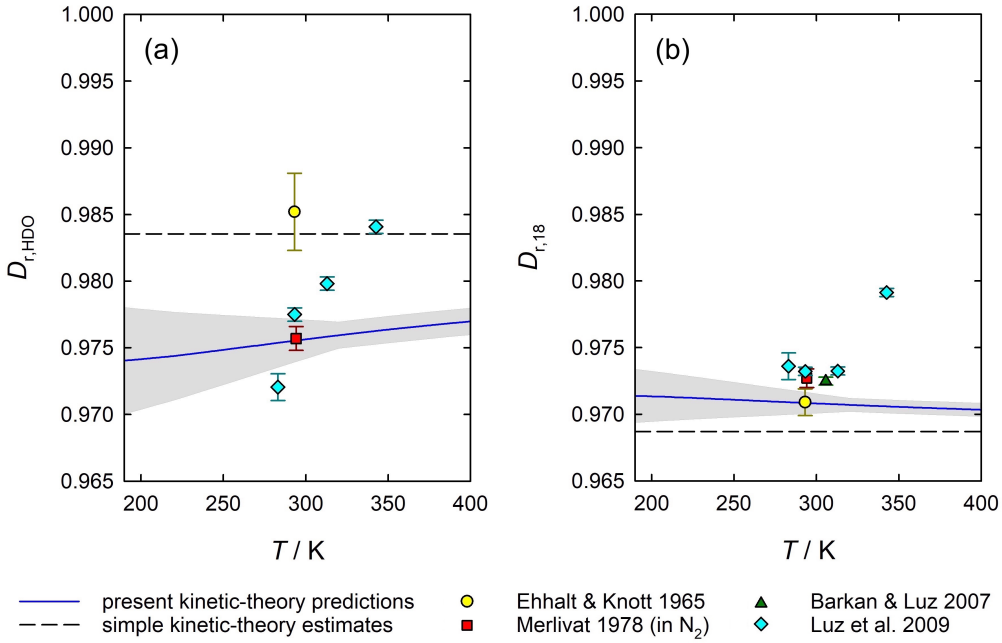


**Figure 3.** Calculated diffusivity ratios $D_{\mathrm{r,HDO}}$ (a) and $D_{\mathrm{r},18}$ (b) in air and available experimental data, as a function of temperature. The shaded areas indicate the estimated expanded uncertainty of the calculations at the 95% confidence level. The figure was taken from the paper of Hellmann and Harvey (2020).

The results for methane diffusion ratios in the $N_2$ atmosphere of Titan, shown in Figure 2, are less surprising. Interactions involving methane are much less anisotropic than those involving water, so one would expect less deviation from hard-sphere results for the $CH_4$–$N_2$ interaction than for the $H_2O$–$N_2$ interaction that is the main component of the water-air system shown in Figure 3. Nevertheless, the mass asymmetry induced by the deuterium substitution in $CH_3D$ is enough to produce a clear temperature dependence and a noticeable difference in $D_{\mathrm{r},CH_3D}$ from the hard-sphere results at low temperatures. As expected, isotopic substitution on the central carbon atom of $CH_4$ has negligible influence on the rotational collision dynamics, producing a diffusivity ratio $D_{\mathrm{r},13}$ nearly indistinguishable from the simple mass-based result of Equation 1.

For convenience in applications, we fitted simple correlating equations to our calculated diffusivity ratios using the symbolic regression software Eureqa (Schmidt & Lipson, 2009). They are valid for temperatures from 100 K to 400 K for $D_{\mathrm{r,HDO}}$, $D_{\mathrm{r},17}$, and $D_{\mathrm{r},18}$ and from 50 K to 200 K for $D_{\mathrm{r},CH_3D}$ and $D_{\mathrm{r},13}$. The resulting expressions are

$$D_{\mathrm{r,HDO}} \equiv D_{\mathrm{HDO}}/D_{\mathrm{H_2O}} = 0.97041 + \frac{0.03842}{(T^*)^{3/4}} - \frac{0.06168}{(T^*)^2} + \frac{0.03010}{(T^*)^3}, \tag{3}$$

$$D_{\mathrm{r},17} \equiv D_{\mathrm{H_2{}^{17}O}}/D_{\mathrm{H_2O}} = 0.98644 - \frac{0.02300}{T^*} + \frac{0.02098}{(T^*)^2} - \frac{0.00470}{(T^*)^4}, \tag{4}$$

$$D_{\mathrm{r},18} \equiv D_{\mathrm{H_2{}^{18}O}}/D_{\mathrm{H_2O}} = 0.97105 - \frac{0.08330}{(T^*)^{3/2}} + \frac{0.08499}{(T^*)^2} - \frac{0.01127}{(T^*)^4}, \tag{5}$$

$$D_{\mathrm{r},CH_3D} \equiv D_{CH_3D}/D_{CH_4} = 0.98379 - \frac{0.00533}{(T^*)^{3/2}} + \frac{0.00143}{(T^*)^4} - \frac{0.00044}{(T^*)^5}, \tag{6}$$

$$D_{\mathrm{r},13} \equiv D_{^{13}CH_4}/D_{CH_4} = 0.98106 - \frac{0.00043}{(T^*)^2} + \frac{0.00059}{(T^*)^3} - \frac{0.00014}{(T^*)^4}, \tag{7}$$

where $T^* = T/(100\ \mathrm{K})$. The correlations reproduce the calculated ratios within $\pm 4 \times 10^{-5}$ and thus well within their uncertainties.

A similar approach could in principle be applied to other planetary atmospheres, but the gas giants would present additional complication. For example, Jupiter has ammonia and water clouds in an atmosphere consisting primarily of hydrogen (Atreya et al., 1999; Young et al., 2019). For water, accurate $H_2O$–$H_2$ potential-energy surfaces exist (Hodges et al., 2004; Valiron et al., 2008; Homayoon et al., 2015). However, the highly quantum nature of $H_2$, and the low temperatures involved, mean that classical trajectory calculations such as those in this paper would likely be significantly in error. Quantitative accuracy would require fully quantum scattering calculations; the framework for such calculations is known (McCourt et al., 1990), but for molecules of this complexity the effort might be prohibitive.

## 4 Conclusion

We have employed state-of-the-art intermolecular potentials for $H_2O$–$CO_2$ and $H_2O$–$N_2$ to perform rigorous kinetic-theory calculations for the diffusivity of water isotopologues in the atmosphere of Mars. The resulting temperature-dependent diffusivity ratios provide the first data for these quantities, enabling the inclusion of kinetic isotope fractionation in future modeling of the hydrologic cycle on Mars. In contrast to similar calculations for diffusivity ratios in Earth's atmosphere, the difference from a simple hard-sphere calculation is at most of only marginal significance.

We performed similar calculations for the diffusion of methane isotopologues in nitrogen, representing the atmosphere of Titan. In that case, a small but not insignificant deviation from the hard-sphere result is obtained for the diffusivity ratio of $CH_3D$.

For convenience in modeling, we have provided temperature-dependent correlations for each diffusivity ratio studied. These are valid from 100 K to 400 K for water in the atmosphere of Mars (Equations 3–5), and from 50 K to 200 K for methane in the atmosphere of Titan (Equations 6 and 7).

In some ways, this paper reports a negative result. The simple hard-sphere theory predicts values almost identical to our more rigorous results for diffusivity ratios of water isotopologues in the Martian atmosphere. However, this negative result is itself unexpected (suggesting some cancellation of errors in the hard-sphere model), because our previous work (Hellmann & Harvey, 2020) demonstrated that the hard-sphere theory is significantly in error for water species in Earth's atmosphere. The difference is marginally significant for $CH_3D$ in Titan's atmosphere, but realistically the effect is probably smaller than other uncertainties would be for any isotopic modeling of Titan in the foreseeable future. However, because these ratios have now been computed, and because Equations 3–7 are simple, the more rigorous diffusivity ratios developed here can be used in modeling with an insignificant increase in computational effort.

**Acknowledgments**

We thank Franck Montmessin for helpful correspondence and Jeffrey Young for helpful review comments. Mention of commercial products in this work is only to specify the procedure used. Such identification does not imply recommendation or endorsement by the National Institute of Standards and Technology, nor does it imply that the products identified are necessarily the best available for that purpose.

## Data Availability Statement

The intermolecular $H_2O$–$CO_2$, $H_2O$–$N_2$, and $CH_4$–$N_2$ potentials used in this study are fully documented in the supporting information of (Hellmann, 2019a, 2019b) and Hellmann et al. (2014). Tables S1 and S2 of the present supporting information provide the calculated diffusivities of $H_2O$, HDO, $H_2{}^{17}O$, and $H_2{}^{18}O$ in $CO_2$, $N_2$, and Mars' atmosphere and the calculated diffusivities of $CH_4$, $CH_3D$, and $^{13}CH_4$ in $N_2$ at a large number of temperatures. The data in Tables S1 and S2 are also provided in the NIST Public Data Repository (Harvey & Hellmann, 2021).

## References


Ádámkovics, M., & Mitchell, J. L. (2016). Search for methane isotope fractionation due to Rayleigh distillation on Titan. *Icarus*, *275*, 232–238. doi: 10.1016/j.icarus.2016.04.006

Armstrong, G. T., Brickwedde, F. G., & Scott, R. B. (1955). Vapor pressures of the methanes. *Journal of Research of the National Bureau of Standards*, *55*(1), 39–52. doi: 10.6028/jres.055.005

Atreya, S. K., Wong, M., Owen, T. C., Mahaffy, P. R., Niemann, H. B., de Pater, I., ... Encrenaz, T. (1999). A comparison of the atmospheres of Jupiter and Saturn: deep atmospheric composition, cloud structure, vertical mixing, and origin. *Planetary and Space Science*, *47*(10), 1243–1262. doi: 10.1016/S0032-0633(99)00047-1

Calado, J. C. G., Lopes, J. N. C., Nunes da Ponte, M., & Rebelo, L. P. N. (1997). Vapor pressure of partially deuterated methanes ($CH_3D$, $CH_2D_2$, and $CHD_3$). *The Journal of Chemical Physics*, *106*(21), 8792–8798. doi: 10.1063/1.473962

Encrenaz, T., DeWitt, C., Richter, M. J., Greathouse, T. K., Fouchet, T., Montmessin, F., ... Ryde, N. (2016). A map of D/H on Mars in the thermal infrared using EXES aboard SOFIA. *Astronomy & Astrophysics*, *586*, A62. doi: 10.1051/0004-6361/201527018

Garberoglio, G., Jankowski, P., Szalewicz, K., & Harvey, A. H. (2018). Fully quantum calculation of the second and third virial coefficients of water and its isotopologues from *ab initio* potentials. *Faraday Discussions*, *212*, 467-497. doi: 10.1039/C8FD00092A

Gat, J. R. (1996). Oxygen and hydrogen isotopes in the hydrologic cycle. *Annual Review of Earth and Planetary Sciences*, *24*, 225–262. doi: 10.1146/annurev.earth.24.1.225

Harvey, A. H., & Hellmann, R. (2021). *Calculated Diffusivities for Water Isotopologues in Carbon Dioxide, Nitrogen, and the Atmosphere of Mars, and for Methane Isotopologues in Nitrogen Representing the Atmosphere of Titan.* National Institute of Standards and Technology, https://doi.org/10.18434/mds2-2351.

Hayes, A. G., Lorenz, R. D., & Lunine, J. I. (2018). A post-Cassini view of Titan's methane-based hydrologic cycle. *Nature Geoscience*, *11*, 306–313. doi: 10.1038/s41561-018-0103-y

Heck, E. L., & Dickinson, A. S. (1996). Transport and relaxation cross-sections for pure gases of linear molecules. *Computer Physics Communications*, *95*(2-3), 190–220. doi: 10.1016/0010-4655(96)00033-1

Hellmann, R. (2019a). Cross second virial coefficient and dilute gas transport properties of the ($H_2O$ + $CO_2$) system from first-principles calculations. *Fluid Phase Equilibria*, *485*, 251–263. doi: 10.1016/j.fluid.2018.11.033

Hellmann, R. (2019b). First-principles calculation of the cross second virial coefficient and the dilute gas shear viscosity, thermal conductivity, and binary diffusion coefficient of the ($H_2O$ + $N_2$) system. *Journal of Chemical & Engineering Data*, *64*(12), 5959–5973. doi: 10.1021/acs.jced.9b00822

Hellmann, R., Bich, E., Vogel, E., & Vesovic, V. (2014). Intermolecular potential energy surface and thermophysical properties of the $CH_4$–$N_2$ system. *The Journal of Chemical Physics*, *141*(22), 224301. doi: 10.1063/1.4902807

Hellmann, R., & Harvey, A. H. (2020). First-principles diffusivity ratios for kinetic isotope fractionation of water in air. *Geophysical Research Letters*, *47*(18), e2020GL089999. doi: 10.1029/2020GL089999

Hellmann, R., & Vogel, E. (2015). The viscosity of dilute water vapor revisited: New reference values from experiment and theory for temperatures between (250 and 2500) K. *Journal of Chemical & Engineering Data*, *60*(12), 3600–3605. doi: 10.1021/acs.jced.5b00599

Hodges, M. P., Wheatley, R. J., Schenter, G. K., & Harvey, A. H. (2004). Intermolecular potential and second virial coefficient of the water–hydrogen complex. *The Journal of Chemical Physics*, *120*(2), 710–720. doi: 10.1063/1.1630960

Homayoon, Z., Conte, R., Qu, C., & Bowman, J. M. (2015). Full-dimensional, high-level *ab initio* potential energy surfaces for $H_2(H_2O)$ and $H_2(H_2O)_2$ with application to hydrogen clathrate hydrates. *The Journal of Chemical Physics*, *143*(8), 084302. doi: 10.1063/1.4929338

Hörst, S. M. (2017). Titan's atmosphere and climate. *Journal of Geophysical Research: Planets*, *122*(3), 432–482. doi: 10.1002/2016JE005240

Krasnopolsky, V. A. (2015). Variations of the $HDO/H_2O$ ratio in the martian atmosphere and loss of water from Mars. *Icarus*, *257*, 377–386. doi: 10.1016/j.icarus.2015.05.021

Marrero, T. R., & Mason, E. A. (1972). Gaseous diffusion coefficients. *Journal of Physical and Chemical Reference Data*, *1*(1), 3–118. doi: 10.1063/1.3253094

McCourt, F. R. W., Beenakker, J. J. M., Köhler, W. E., & Kuščer, I. (1990). *Non-Equilibrium Phenomena in Polyatomic Gases*. Oxford: Clarendon Press.

Mitchell, J. L., & Lora, J. M. (2016). The climate of Titan. *Annual Review of Earth and Planetary Sciences*, *44*, 353–380. doi: 10.1146/annurev-earth-060115-012428

Montmessin, F., Fouchet, T., & Forget, F. (2005). Modeling the annual cycle of HDO in the Martian atmosphere. *Journal of Geophysical Research: Planets*, *110*(E3), E03006. doi: 10.1029/2004JE002357

Neese, F. (2012). The ORCA program system. *WIREs Computational Molecular Science*, *2*(1), 73–78. doi: 10.1002/wcms.81

Niemann, H. B., Atreya, S. K., Demick, J. E., Gautier, D., Haberman, J. A., Harpold, D. N., ... Raulin, F. (2010). Composition of Titan's lower atmosphere and simple surface volatiles as measured by the Cassini-Huygens probe gas chromatograph mass spectrometer experiment. *Journal of Geophysical Research: Planets*, *115*(E12), E12006. doi: https://doi.org/10.1029/2010JE003659

Nixon, C. A., Temelso, B., Vinatier, S., Teanby, N. A., Bézard, B., Achterberg, R. K., ... Flasar, F. M. (2012). Isotopic ratios in Titan's methane: Measurements and modeling. *The Astrophysical Journal*, *749*(2), 159. doi: 10.1088/0004-637x/749/2/159

O'Connell, J. P., Gillespie, M. D., Krostek, W. D., & Prausnitz, J. M. (1969). Diffusivities of water in nonpolar gases. *The Journal of Physical Chemistry*, *73*(6), 2000–2004. doi: 10.1021/j100726a059

Roe, H. G. (2012). Titan's methane weather. *Annual Review of Earth and Planetary Sciences*, *40*, 355–382. doi: 10.1146/annurev-earth-040809-152548

Schmidt, M., & Lipson, H. (2009). Distilling free-form natural laws from experimental data. *Science*, *324*(5923), 81–85. doi: 10.1126/science.1165893

Stanton, J. F., Gauss, J., Cheng, L., Harding, M. E., Matthews, D. A., & Szalay, P. G. (2019). *CFOUR, Coupled-Cluster techniques for Computational Chemistry, a quantum-chemical program package. Version 2.1. For the current*

*version, see http://www.cfour.de.*

Thelen, A. E., Nixon, C. A., Cordiner, M. A., Charnley, S. B., Irwin, P. G. J., & Kisiel, Z. (2019). Measurement of $CH_3D$ on Titan at submillimeter wavelengths. *The Astronomical Journal*, *157*(6), 219. doi: 10.3847/1538-3881/ab19bb

Trainer, M. G., Wong, M. H., McConnochie, T. H., Franz, H. B., Atreya, S. K., Conrad, P. G., ... Zorzano, M.-P. (2019). Seasonal variations in atmospheric composition as measured in Gale Crater, Mars. *Journal of Geophysical Research: Planets*, *124*(11), 3000–3024. doi: 10.1029/2019JE006175

Valiron, P., Wernli, M., Faure, A., Wiesenfeld, L., Rist, C., Kedžuch, S., & Noga, J. (2008). R12-calibrated $H_2O$–$H_2$ interaction: Full dimensional and vibrationally averaged potential energy surfaces. *The Journal of Chemical Physics*, *129*(13), 134306. doi: 10.1063/1.2988314

Villanueva, G. L., Mumma, M. J., Novak, R. E., Käufl, H. U., Hartogh, P., Encrenaz, T., ... Smith, M. D. (2015). Strong water isotopic anomalies in the martian atmosphere: Probing current and ancient reservoirs. *Science*, *348*(6231), 218–221. doi: 10.1126/science.aaa3630

Vos, E., Aharonson, O., & Schorghofer, N. (2019). Dynamic and isotopic evolution of ice reservoirs on Mars. *Icarus*, *324*, 1–7. doi: 10.1016/j.icarus.2019.01.018

Young, R. M. B., Read, P. L., & Wang, Y. (2019). Simulating Jupiter's weather layer. Part II: Passive ammonia and water cycles. *Icarus*, *326*, 253–268. doi: 10.1016/j.icarus.2018.12.002